

Origin of characteristic subgap optical absorption in CVD diamond films

M. Nesládek, K. Meykens, and L. M. Stals

*Materials Physics Division, Institute for Materials Research, Limburgs Universitair Centrum,
Wetenschapspark, B-3590 Diepenbeek, Belgium*

M. Vaněček and J. Rosa

*Institute of Physics, Academy of Sciences of the Czech Republic, Cukrovarnicka 10, CZ-162 00 Prague, Czech Republic
(Received 25 September 1995; revised manuscript received 16 April 1996)*

Photothermal deflection spectroscopy (PDS) is used to study subgap optical absorption in chemical vapor deposited (CVD) diamond films. The high PDS sensitivity over a broad investigated spectral range enabled the investigation of the main defect structure in CVD diamond upon changing the deposition conditions. All films exhibit a very characteristic shape of the subgap optical absorption in the infrared and visible spectral regions, which scales with the content of amorphous carbon phase in grain boundaries. In best-quality films the character of the fundamental absorption edge is attained and the subgap absorption reduced. For nanocrystalline approaching films, an absorption spectrum resembling closely the one for amorphous carbon (*a*-C:H) films is observed. Based on these results a mathematical model for the description of the optical absorption coefficient in the subgap region is developed. A numerical deconvolution procedure is applied to fit the experimental data. [S0163-1829(96)08331-2]

I. INTRODUCTION

Diamond as a covalently bonded wide-band-gap semiconductor has been widely studied, but only recent developments in the chemical vapor deposited (CVD) technology opened up new possibilities for the preparation of thin-film devices and for new extensive research activities in this field.¹⁻³ Recently, it has been shown that in some homoepitaxially grown CVD diamond films the charge carrier mobilities start to approach values found for natural diamond.³⁻⁵ Nevertheless, tested devices perform rather modestly⁴ in comparison with the existing ones, based on Si, Ge or III-V, II-VI materials. One of the key issues in the preparation of high-quality CVD diamond films is the defects and a deeper understanding of their localized defect states in the band gap is needed for further progress to be made in the CVD diamond-electronics field.

Defects, classified generally as *N*, *GR*, *R*, *TR*, *H*,⁶ have been thoroughly investigated in the past in natural and high-pressure high-temperature (HPHT) synthetic diamond. Many of these defects are related to the presence of nitrogen, which is the main extrinsic impurity in diamond. The defects and their electronic models are discussed in detail in the literature.⁶⁻¹⁰ In this paper we concentrate on defects in CVD films. Recently, we showed that CVD films exhibit a characteristic subgap continuum absorption,¹¹ not observed for natural or HPHT synthetic diamond.

Specific of the low-pressure CVD diamond is the preparation in the pressure-temperature region, in which graphite is thermodynamically stable over diamond. This fact may account for the observed differences. One possibility to consider is the presence of π -bonded carbon. Thermodynamic growth models,¹²⁻¹⁴ based on the preferential etching of the nondiamond phase and/or diamond surface stabilization by atomic hydrogen, always include a certain probability for the incorporation of sp^2 carbon in the diamond films. sp^2 sites

play an essential role in amorphous carbon (*a*-C:H) or higher-ordered tetrahedrally bonded amorphous carbon (*ta*-C) films. It is widely accepted that in *a*-C:H π -bonded carbon atoms cause the formation of a π - π^* pseudogap, emerging about midgap (in between the σ - σ^* bands) and dominating the optical absorption.¹⁵⁻¹⁷ Similarly to *a*-C:H and *ta*-C, the *D* (disorder) and *G* (graphite) Raman scattering bands are present^{18,19} in lower-quality diamond films.

Optical absorption methods have proven to be very powerful for studying the electronic structure in tetrahedrally bonded semiconductors.²⁰⁻²² When looking for defect-induced subgap absorption in the ppm (parts per million) range and lower, as is required for an electronic-quality material, very sensitive techniques must be used. In commercial spectrophotometers absorbance values down only to the 10^{-2} level can be measured. Moreover, light scattering in CVD diamond films (due to bulk inclusions and to grain boundaries in polycrystalline films) make standard transmission measurements difficult.²³

To study the defect-induced optical absorption in CVD diamond we recently applied photothermal deflection spectroscopy (PDS).^{11,24-26} This method made it possible to measure absorbances down to a 10^{-5} level, and thus to investigate deep defects on a ppm scale and below, even in 10- μ m-thick diamond films.¹¹ The main aim of this paper is to report in detail on the characteristic subgap continuum absorption in CVD diamond films deposited under various conditions and to compare their absorption with the known absorption spectra of type IIa (natural) and type Ib (HPHT) diamond.

In Sec. IV of this paper we develop a theoretical model for the description of the defect induced optical absorption in CVD diamond. We show that the optical absorption coefficient can be fitted to the experimental data when considering optical transitions due to the presence of π -bonded carbon in the grain boundaries.

TABLE I. The deposition conditions for samples of sets I (constant temperature) and II (constant methane concentration). Summarized are also the characteristics of samples and the ratio of intensities $I(D)/I(G)$ of D (disorder) and G (graphite) Raman peaks at full width at half maximum (FWHM).

Sample	Pressure (Pa)	Temp. (K)	CH4 (%)	MW power (W)	Depos. time (min)	Appearance	Morphology	Grain size (μm)	$I(D)/I(G)$ at FWHM Raman peaks
d2.1	6600	1173	0.65	800	720	White	Random	5	No G peak ^a
d2.2	6600	1173	1	800	720	Gray	Random	3	≈ 5
d2.3	6600	1173	1.5	800	720	Gray	Random	3	≈ 1
d2.4	6600	1173	2	800	720	Brownish	Nanocrystalline	< 1	≈ 0.2
d2.6	6600	1173	2.5	800	720	Brownish	Nanocrystalline	< 0.1	Only G
d2.7	6600	1093	3	800	720	Gray	Nanocrystalline	< 1	≈ 0.2
d2.8	6600	1033	3	800	720	Gray	{100}	≈ 2	≈ 0.5
d2.9	6600	1173	3	800	720	Dark brown	Nanocrystalline	< 0.1	Only G
D11	13 200	1033	3 ^b	4000	1440	White	Random	15	No G peak ^a

^a1332 cm^{-1} peak only.

^bAlso 1 sccm (cubic centimeter per minute at standard temperature and pressure) O_2 .

II. EXPERIMENTAL DETAILS

A. Diamond samples

Diamond films were grown by means of plasma-enhanced chemical vapor deposition in an ASTEX PDS-17 microwave plasma reactor. Undoped Si wafers were used as substrate material. Care was taken to maintain a low background pressure in the vacuum vessel before starting the deposition and about the cleanness of the reactor walls, to reduce the incorporation of extrinsic impurities in the deposited films. The deposition processes consisted of two consecutive steps: (1) the bias-enhanced nucleation step^{27,28} for creating a sufficiently high diamond nucleation density (10^{10} cm^{-2}) on a mirror polished Si substrate; (2) the growth step. The deposition parameters of sets I (constant temperature) and II (constant methane concentration) are summarized in Table I.

The main experimental interest was to find out how π -bonded carbon can be incorporated into CVD diamond films. Because one possible site for amorphous carbon are grain boundaries^{18,29–32} we attempted to change their area by changing the film morphology. By keeping the nucleation step constant and changing the growth-step deposition conditions various film morphologies were prepared, ranging from those containing well-defined crystals to those showing a finely grained morphology. The characteristics of the deposited films are summarized in Table I. We attempted to compare the optical absorption of these films with our best film (D11), prepared at the optimized conditions.¹¹ The samples D11 and d2.1 only exhibited the Raman diamond peak at 1332 cm^{-1} . All other films exhibited a typical broad feature at 1550 cm^{-1} in the Raman spectra (G peak) varying in intensity (see Table I).

The growth rate was typically 1.5 $\mu\text{m}/\text{h}$, and films with a thickness between 15 and 20 μm were deposited (with the exemption of the film D11, which was prepared under different conditions and which was 100 μm thick). After the deposition the diamond films had to be removed from the substrates to allow the PDS measurements. Therefore, the Si substrate was etched away in a $\text{HNO}_3/\text{HF}/\text{H}_2\text{O}$ mixture and traces of surface graphitic carbon were removed in a $\text{H}_2\text{SO}_4/\text{CrO}_3$ solution.

Bulk type IIa (natural) and Ib (HPHT) DeBeers monocrystalline diamond plates 250 μm thick and also a {100}-oriented homoepitaxial diamond (sample D17) deposited on IIA DeBeers plate were used for comparison.²⁶

B. Optical characterization

Self-supporting CVD diamond films of dimensions typically $4 \times 4 \text{ mm}^2$, $2 \times 2 \text{ mm}^2$ type IIa, and Ib monocrystalline diamond plates and homoepitaxial diamond films deposited on $2 \times 2 \text{ mm}^2$ type IIa diamond plates were used for the optical absorption measurement by use of PDS.

The principle of PDS is the following: A high-intensity light beam from a monochromator (pumping beam) is modulated by a mechanical chopper and focused on the diamond film, which is immersed in spectroscopically pure CCl_4 . Photons absorbed in the film cause a temperature elevation in the illuminated area. The thermal wave generated in the CVD diamond film propagates into CCl_4 and modulates the index of refraction of the CCl_4 liquid.^{33–35} A He-Ne laser beam, directed parallel and as closely as possible to the sample surface (probe beam) is periodically deflected, the deflection $\Delta\varphi$ being proportional to the absorptance A of the measured thin film and the pumping beam intensity. The deflection $\Delta\varphi$ is detected by a silicon position sensitive four quadrant diode^{33–35} as a small ac voltage signal (PDS signal S), proportional to $\Delta\varphi$. The PDS signal S is measured by a lock-in amplifier. By scanning the wavelength of the monochromatic pump beam from the region of complete light absorption in the film (e.g., the saturation of PDS signal $S = S_{\text{sat}}$ is reached) to the region of low absorption, a full PDS spectrum is obtained.

Full details of the experimental setup^{11,25,33–35} and the evaluation procedure^{11,25,33–35} for the calculation of the optical absorption coefficient α can be found elsewhere. Here, only the details,^{11,25,36} important for the measurement of CVD diamond thin films are given. It is important to note that the effect of light scattering in the bulk or at the rough surface of CVD diamond films is much less significant for PDS than for conventional transmission measurements, be-

cause just the light scattered (and absorbed) in the direction of the probe beam gives some contribution to the PDS signal.

Under typical experimental conditions (chopping frequency 14 Hz, sample thickness 20–200 μm , spectral resolution of the monochromator 8 nm) the PDS signal S , normalized to a constant pumping beam intensity, can be written in the incoherent limit^{34,35} as

$$S = S_{\text{sat}}[1 - \exp(-\alpha d)], \quad (1)$$

where S_{sat} is the saturated signal in the spectral region where a full absorption occurs, d is the sample thickness, and α is the optical absorption coefficient. The reflectance is assumed to be approximately spectrally independent in the investigated spectral range.³⁷ Some films (d2.6, d2.9 see Table I) showed a saturation of the PDS signal S_{sat} in the investigated spectral range. For these films the optical absorption was directly calculated using Eq. (1). For the samples of which the saturation signal was not reached in the investigated spectral range (d2.1, d2.4, d2.7, d2.8), the following procedure was used: all parameters of the experimental setup were kept the same, hence, the proportionality coefficient^{34,35} S_{sat} between the probe beam deflection $\Delta\varphi$ and the PDS signal S in Eq. (1) remains the same. In the high-quality diamond sample D11 (see Table I) the optical transmission and reflection were measured using a Perkin-Elmer Spectrophotometer, equipped with a light-integrating sphere. These data were used as a cross check for the proportionality coefficient value in a higher photon energy (E) part of the spectrum. In a low absorption region the optical absorption coefficient α was determined from the PDS signal S , using the above described procedure.

To reduce the experimental noise, a 1-mW He-Ne laser with a high pointing stability and an optimized beam geometry was used, focused as closely as possible to the smooth side of the diamond film (the side of the Si/diamond interface after the chemical etch). Care was taken to reduce vibrations of the experimental setup and to avoid scattering of the laser beam optical path in air and in the transparent deflection liquid (CCl_4) due to particulates. Additionally, a long black tube was placed in front of the position sensor to stop ambient scattered light modulated at the chopper frequency and to define a narrow field of view, just letting pass the probing He-Ne laser beam. The whole apparatus was computer controlled and typically 300 readings of the lock-in amplifier were averaged at each photon energy.

III. RESULTS AND DISCUSSION

A. Twinning and development of texture

As the main objective was to trace the development of characteristic defects in CVD diamond while changing the deposition conditions, there was particular interest in investigating films containing various amounts of sp^2 carbon (see Table I).

The surface morphology of investigated films is shown in our previous work.²⁵ To summarize, at low methane concentrations (samples d2.1, d2.2, d2.3), films were white and/or translucent (light scattering) and nontextured. As the methane concentration increased the films became very finely grained and they were brown and optically smooth. Surpris-

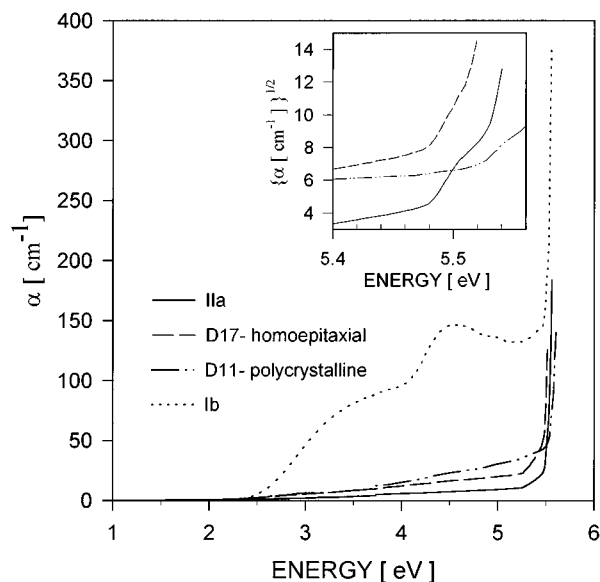


FIG. 1. The optical absorption coefficient α for 100- μm -thick polycrystalline sample D11, for 373- μm -thick {100}-oriented sample D17, and for type Ila (natural) diamond and type Ib (high-pressure high-temperature synthetic) diamond plates, calculated from the optical transmission measurements. The inset shows the indirect optical transitions at the fundamental absorption edge of diamond.

ingly, reduction of the substrate temperature again led to the deposition of films with defined grain sizes, and approaching the {100} morphology.

Twinning³⁸ must be at least partially responsible for the development of the observed finely grained film morphology (samples d2.4, d2.6, d2.7, d2.9). If only a drift from the diamond deposition domain³⁹ causes the development of the finely grained morphology, a reduction of the deposition temperature would not restore regular crystal shapes (sample d2.8). Similar conclusions about the influence of the twinning on successively smaller areas were recently drawn by Tamor and Everson.⁴⁰

Stacking or multiple stacking faults are very often found in diamond films.^{38,40} This is not surprising because the energy difference for the correct and incorrect hexagonal ring stacking (staggered to eclipsed) is very small. On the atomic scale, twinning means in-plane incorporation of the boat type six-membered rings instead of an incorporation of the correct chair ring type. When the film grows these two cases differ only in the next-nearest-neighbor environment.³⁸ In case of a very small misorientation between crystallites a bond-angle disorder can be induced to bond adjacent crystals. It appears likely that for crystallites with higher misorientations, amorphous carbon regions on grain boundaries can be produced to reduce the total energy of the system. The amorphous carbon on grain boundaries was experimentally confirmed by various techniques such as Raman spectroscopy and electron-energy-loss spectroscopy.^{30–32}

B. Optical measurements

1. Transmission measurements

In Fig. 1 the optical absorption coefficient α , calculated

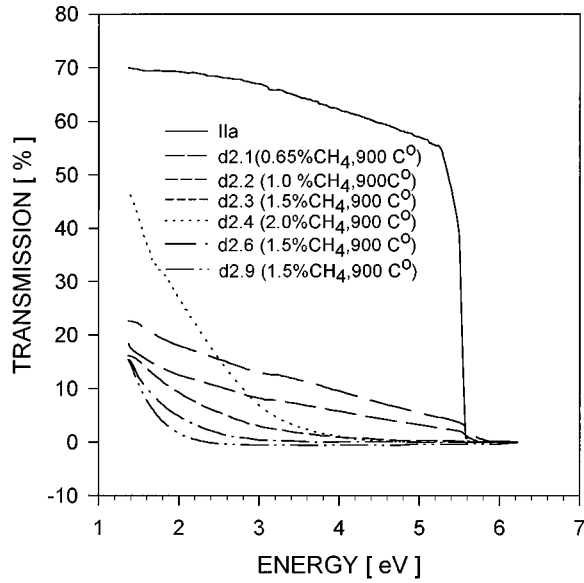


FIG. 2. The optical transmission spectra (without correction for the elastic light scattering) of samples prepared at various methane concentrations and at a constant substrate temperature of 900 C° (set I). Transmission of Ila diamond plate is shown for comparison.

from the optical transmission measurements, for the polycrystalline sample D11, homoepitaxial layer D17, and type Ila and type Ib diamond plates is plotted. Ila diamond shows a typical indirect absorption edge at 5.45 eV. This absorption can be described by the $\alpha \approx (E - E_g \pm E_{ph})^2$ dependence for parabolic bands²² (see the inset of Fig. 1). Similarly, it was found by Sussmann and *et al.*⁴¹ that the UV absorption spectra for polished high-quality CVD films approach those for Ila diamond. The homoepitaxially grown diamond (D17) and the best polycrystalline material (D11) attain the character of the fundamental absorption edge, but a broadening, especially for polycrystalline material, can be clearly observed in Fig. 1. It should be noted that, because the absorption coefficient falls off sharply in this region, light scattering at grain boundaries cannot cause the broadening, as proved by modeling.

The absorption in the high-quality CVD diamond film D11 attains the character of the fundamental absorption edge. This statement is not true for all CVD films. Figures 2 and 3 show the optical transmission data between two limiting cases: first (samples d2.1, d2.2), following the optical transmission of Ila diamond (measured without the integration sphere), but with much lower detected transmission because of the scattering losses and, second, a slowly decaying transmission from the energy corresponding to the expected band edge for diamond. Similar tailing of the optical absorption coefficient into the band gap was also observed for α -C:H films.^{42,43}

2. PDS measurements

To study the weak subgap absorption the PDS measurements were performed, shown in Figs. 4 and 5. In Fig. 4 the optical absorption coefficient α of our best polycrystalline material (D11) is plotted and compared with the optical absorption coefficient for Ila diamond.²⁵ The absorption in Ila diamond (investigated only in the 1–3-eV region) is just

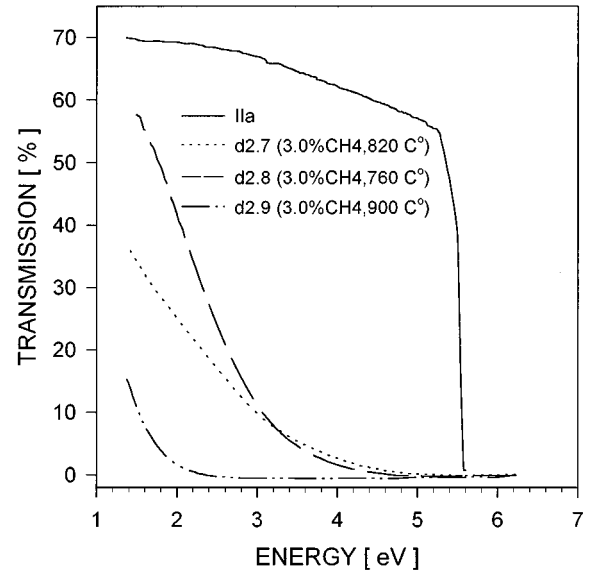


FIG. 3. The optical transmission spectra (without correction for the elastic light scattering) of samples prepared at a methane concentration of 3% and at various substrate temperatures (set II).

above the detection limit of the PDS apparatus used. The polycrystalline diamond shows a distinct optical absorption in the subgap region.

The optical absorption of the samples from the sets I and II is shown in Fig. 5. It can be seen that all these samples also show the characteristic spectral dependence of the optical absorption coefficient α .²⁵ The absolute value of the optical absorption coefficient increases with the nondiamond carbon content (the closer to nanocrystalline films the higher

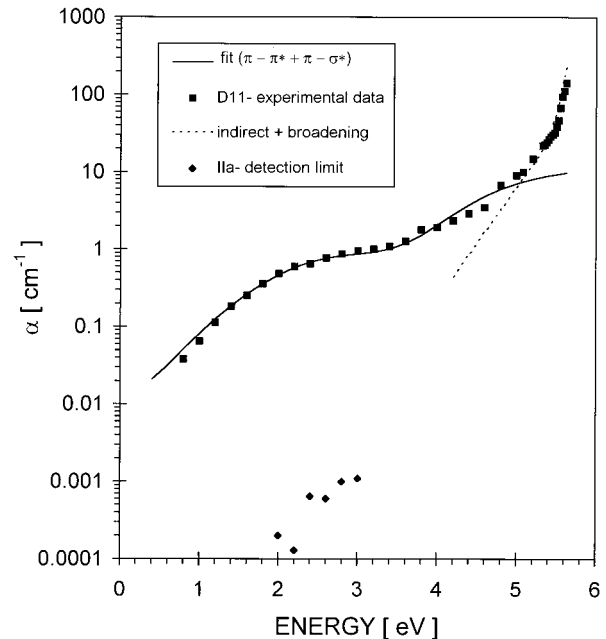


FIG. 4. The spectral dependence of the optical absorption coefficient α obtained from PDS measurements for the film D11 and for the bulk Ila diamond sample (investigated only in the range 1–3 eV). Plotted are also numerical fits to Eq. (2) (π - π^* and π - σ^* transitions) and to Eq. (8) (indirect transitions and exponential broadening), discussed in Sec. IV.

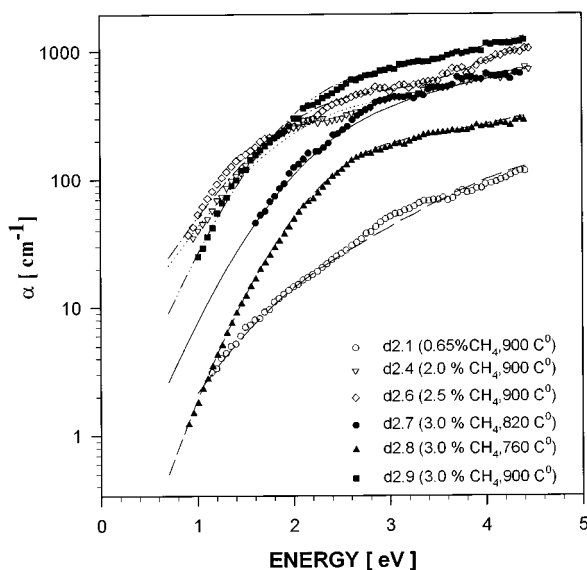


FIG. 5. The spectral dependence of the absorption coefficient α obtained from PDS measurement for the films of set I (samples differ in CH_4 concentration in the H_2 feed gas during deposition) and for the films of set II (samples are deposited at different substrate temperatures). Plotted are also numerical fits to Eq. (2).

the absorption) and the saturation of the PDS signal S occurs at lower photon energy, for the same sample thickness. For the better quality samples (d2.1, d2.8) with the regular crystal morphologies the subgap absorption is reduced.

Photocurrent measurements in polycrystalline CVD diamond films⁴⁴ showed a similar type of spectral dependence as the optical absorption measurements presented in this work. It has been suggested that the optical transitions involved are due to the presence of an electronic level 1 eV distant from the valence-band edge.

According to the development of the absorption spectra when continuously changing the deposition conditions (and correspondingly developing the finely grained morphology) and according to a close similarity of the measured absorption spectra with the absorption spectra of α -C:H films^{17,42,43} we propose that the π - π^* band-type transitions are responsible for the observed absorption. The model of the π - π^* pseudogap was originally developed by Roberston and O'Reilly¹⁵ and Bredas and Street¹⁶ for amorphous carbon. Recently, photoluminescence studies in polycrystalline CVD diamond accompanied with micro-Raman measurements attributed the observed broadband luminescence, centered about 2 eV, to amorphous carbon in grain boundaries.^{30,31}

Nitrogen related absorption in CVD diamond films was investigated recently.^{25,26} A typical absorption spectrum due to substitutional nitrogen in type Ib HPHT diamond is shown in Fig. 1. Investigated films show a clearly different spectral dependence of the optical absorption coefficient compared to Ib diamond.

Secondary-ion-mass spectroscopy (SIMS) analysis²⁵ shows typically 30 ppm N, 500 ppm H, and 100 ppm O in the undoped films investigated in this study. The subgap absorption varies for the measured samples by 4 orders of magnitude. So it is difficult to explain the observed spectra by impurity absorption.

3. Light scattering

In this section, we would like to show that the typical shape of the optical absorption in the films, measured in this work, cannot be due to elastic light scattering. The spectral dependence of the optical scattering coefficient should then indeed be dramatically changed in going from large grain sized films to optically smooth nanocrystalline films (e.g., from Mie-type scattering on large defects as grain boundaries to Rayleigh-type scattering due to defects on a microscopical scale). These two scattering types have quite different spectral dependencies.⁴⁵

Further, it follows from its operation principle that PDS is much less sensitive to optical scattering than transmission measurements³³ because the contribution of scattered light to the PDS signal comes only from the scattered pump-beam light in the direction along the He-Ne probe beam. If the sample is strongly light scattering and weakly absorbing in the infrared and visible parts of the spectrum (as the high-quality sample D11 in Fig. 4) and if we use the usual way of setting the PDS signal to the absolute scale with the help of the saturated PDS signal value³³⁻³⁵ then the absorption coefficient in a low absorption region can be overestimated. This has been observed for amorphous silicon thin films deposited on rough glass substrates. The reason is that a relative contribution of the scattered light is higher in the low absorption region but negligible in the saturation region (strongly absorbed light does not penetrate through the film towards the light-scattering surface). For large-grain sized films we partly overcame this problem by setting the PDS spectrum on the absolute scale with the help of the transmittance-reflectance measurement using the light-integration sphere. For optically smooth homoepitaxial and finely grained films (d2.9, etc.) the effect is negligible.

To summarize, the main support that the typical spectral dependence of subgap absorption is not substantially influenced by the light scattering comes from the fact that all investigated films, ranging from rough to very smooth, show the similar spectral shape of the optical absorption coefficient α in the 0.9–3-eV region. This absorption is shifted just for various films on the absolute scale. We observe a higher subgap absorption in the optically smooth, nonscattering films.

IV. MODEL OF THE OPTICAL ABSORPTION IN CVD DIAMOND

Based on the above presented experimental results it can be concluded that there is enough evidence to suggest that the main defect structure (dominating the defect-induced optical absorption in polycrystalline diamond films) is associated with π -bonded carbon.

In-plane bonded six-membered hexagonal rings with 120° bonding angle between each C atom exist in pure graphite. Their incorporation into the diamond structure with 109.5° tetragonally bonded C would lead to an enormous distortion. A much more probable explanation was presented in Sec. III. This is that amorphous carbon is located mainly in grain boundaries and at other defects. It is interesting to note that already some time ago π -bonded carbon clusters were suggested as an explanation of the optical absorption induced by radiation damage in IIa diamond.⁴⁶

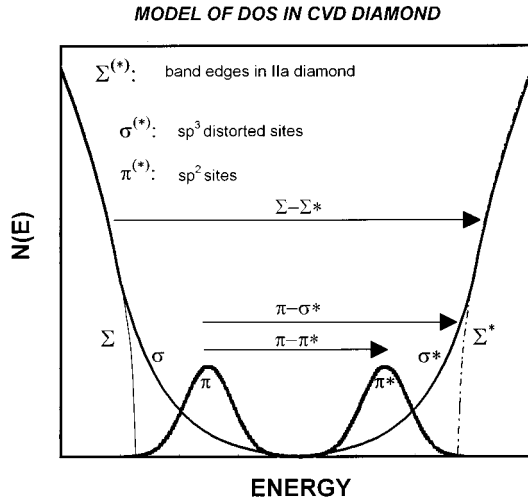


FIG. 6. The schematic model of the density of states in the gap of CVD diamond, discussed in Sec. IV. The π and π^* bands appear due to the presence of amorphous carbon regions. Shown are also two parabolic bands Σ, Σ^* for diamond and the exponentially broadened tails σ, σ^* (starting at the energy E_m). Optical transitions are marked by arrows.

Various models of optical absorption, such as those based on theories of Tauc,²⁰ Abe and Toyozawa,⁴⁷ and others were developed to describe the optical absorption in materials retaining only short-range order such as amorphous silicon (a -Si) and amorphous hydrogenated silicon (a -Si:H). For amorphous carbon the situation is more complex because of the mixed π - σ bonding environment. Theoretical considerations for possible optical transitions in a -C:H were discussed by Robertson,¹⁷ based on the Tauc model of a virtual crystal. In Tauc's model²⁰ only the conservation of energy and no conservation of momentum is assumed. The momentum matrix elements T are then replaced by their average value T_0 .²² Upon assuming the Velicky summation rule²² the optical absorption coefficient α can be written as

$$\alpha(E) = CE^{-1} \int g_i(\epsilon) f(\epsilon) g_f(\epsilon+E) [1-f(\epsilon+E)] d\epsilon, \quad (2)$$

where g_i and g_f are the initial and final density of states, respectively, $f(\epsilon)$ and $f(\epsilon+E)$ are the Fermi-Dirac occupation functions for the initial and final states and the constant C is proportional to the momentum matrix elements T_0^2 . The approximate spectral independence of the matrix elements was experimentally confirmed for a -Si:H by Jackson *et al.*⁴⁸

Our model of the subgap optical transitions is based on the currently accepted electronic picture of amorphous carbon¹⁷ and on recent molecular-dynamics simulations, showing the presence of π, π^* states in the computed electronic density of states.^{49,50} Our model is shown in Fig. 6. The following transitions are considered: (1) π - π^* (Gaussian bands) transitions in amorphous carbon regions. (2) π - σ^* transitions in amorphous carbon regions. (3) Indirect transitions between the valence and conduction bands of diamond.

As shown in the following sections, an independent value for the preintegration factor in Eq. (2) is considered for each

of these optical transitions to include the fact that the value of the optical matrix elements associated with each particular optical transition can be different.

A. π - π^* transitions

The origin of the pseudogap in a -C:H and highly-ordered materials, such as tetrahedrally bonded amorphous carbon (ta -C), is still subject to discussion.⁴⁹⁻⁵⁴ The molecular-dynamics study of Wang, Ho, and Chan⁵¹ suggested that graphitic clusters are arranged in planar sheets, containing mostly 6- and some 5- or 7-membered rings. It has been proposed that in highly-ordered structures the clustering of aromatic rings will not be energetically favorable. Recently Stephan *et al.*⁵⁰ suggested that with increasing atomic density the number of fused rings decreases. For dense films, the existence of single rings, or pairs, or single defects is favored. This idea was supported by Drabold, Fedders, and Strum,⁵² who introduced π -bonded defect pairs as the main defect. Recently, it was shown⁵⁴ in the framework of the tight-binding Huckel Hamiltonian that a single, distorted aromatic ring, forming a boat or chair configuration and consequently causing π - σ mixing, can produce states lying close to the midgap in ta -C.

In our model, the localized π band is approximated by a statistical Gaussian distribution of the density of localized states, centered at E_i ($i=1,2$) and with a half-width $2w$. Both π and π^* bands are taken as symmetrical around the midgap, as expected from recent molecular-dynamics simulations.⁴⁹ The π ($i=1$) and π^* ($i=2$) band density of states are

$$g_{i(i=1,2)}(\epsilon) = A(2\pi w^2)^{-1/2} \times \exp[-(\epsilon - E_i)^2/2w^2]. \quad (3)$$

The convolution integral Eq. (2) can then be solved analytically, leading to the expression for the optical absorption coefficient $\alpha_{\pi\pi^*}$:

$$\alpha_{\pi\pi^*}(E) = A^2(2E\pi w^2)^{-1} \int \exp[-(\epsilon - E_1)^2/2w^2] \exp[-(\epsilon - E_2)^2/2w^2] d\epsilon \quad (4)$$

and after integration (A and B_1 are constants),

$$\begin{aligned} \alpha_{\pi\pi^*}(E) &= A^2(2E\sqrt{\pi})^{-1} \exp[-(E_{\pi\pi^*} - E)^2/4w^2] \\ &= B_1 E^{-1} \exp[-(E_{\pi\pi^*} - E)^2/4w^2]. \end{aligned} \quad (5)$$

Equation (5) has a clear interpretation. The convolution integral reaches its maximum for a photon energy equal to the energy distance between two symmetrical π - π^* density of states distributions. The final joint density of states is again a Gaussian distribution but with a half-width of $4w$. The optical absorption coefficient, calculated according to Eq. (5), is plotted for various values of w and E_0 ($=E_1 - E_2$) in Fig. 7. The similarity between the spectra in Fig. 7 and the experimental data, presented in Fig. 5, and the data measured by Bounough *et al.*⁴³ and by Veerasamy *et al.*⁵⁵ for a -C:H suggests the validity of our model for the π - π^* transitions.

The fit of the experimental subgap absorption spectra (see Sec. IVD and Figs. 4 and 5) using the model based on the

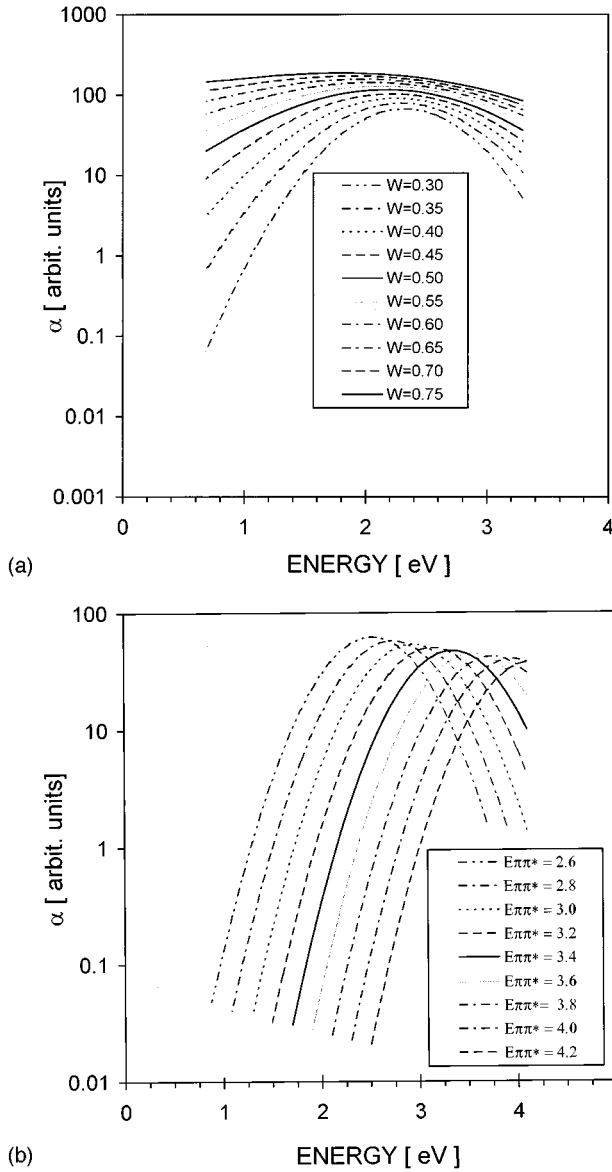


FIG. 7. Numerical calculation of the optical absorption coefficient α according to Eq. (5) due to π - π^* transitions, described by the parameters $w, E_{\pi\pi^*}, B_1$. Simulations are shown for different values (w); $E_{\pi\pi^*}$ is set to 3.5 eV in these calculations (a), and simulations for various values of $E_{\pi\pi^*}$ (see also Fig. 6); w is set to 0.5 eV (b).

Eq. (5) yields a very good agreement for all films, ranging from nanocrystalline to well-faceted diamond films. Practically, the main difference between fitting parameters is the value of constant B_1 in Eq. (5), which is proportional to the product of the optical matrix elements and the concentration prefactor of π and π^* distributions of states [Eq. (3)]. The fit yields typically 3.5 eV for energy distance between the two maxima of the π - π^* distributions $E_{\pi\pi^*}$ for investigated CVD diamond films. The molecular-dynamics simulations⁴⁹ suggested a value between 4 and 5 eV for $E_{\pi\pi^*}$ in tetrahedrally bonded amorphous carbon. In Fig. 8 we plot the value of optical absorption coefficient α at 3.5 eV as a function of the preintegration constant B_1 , obtained from Eq. (5) by using the least-square fitting procedure. It can be seen that the $\alpha(B_1)$ dependence has a linear character as expected from

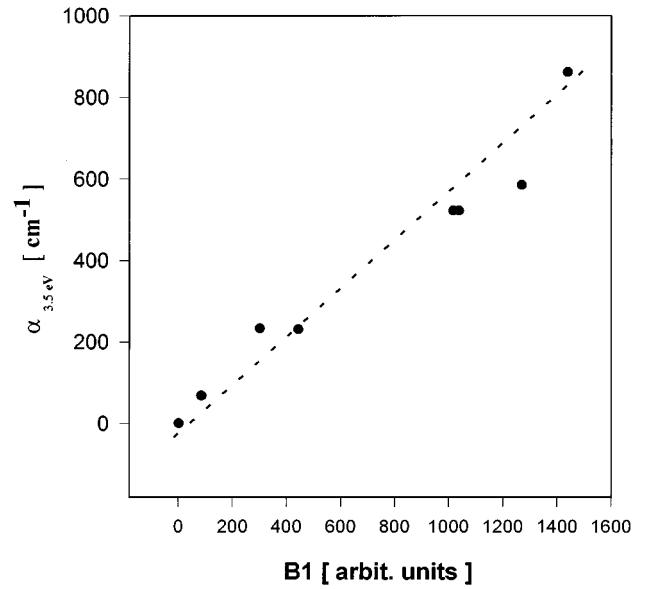


FIG. 8. The plot of the value of the optical absorption coefficient α at 3.5 eV for films from Figs. 4 and 5 as a function of the preintegration constant B_1 from Eq. (5), obtained by numerical fitting procedure.

Eq. (5) and supporting our model.

It should be noted that this approximation is different from the approach used frequently in the literature for a -C:H, where the Tauc plot, approximating the optical transitions between two parabolic bands in amorphous semiconductors, is used to fit experimental data.

B. π - σ^* transitions

It has been suggested that localized-localized state π - π^* transitions are allowed, if they occur with the initial and final states localized on the same cluster.¹⁷ The π - σ^* transitions would be possible if π - σ bond mixing in amorphous carbon regions occurs. Bond-angle distortions due the immersing the sp^2 atoms in the sp^3 environment were suggested in recent molecular-dynamics work.^{49,50} Because, the sp^2 sites are neighboring the sp^3 sites, a sufficient bonding angle distortion could enhance the π - σ^* optical transitions. This allows one to use the same approximation as in Sec. IV A for the calculation of the optical absorption coefficient α [Eq. (2)] but with a different preintegration factor. This is in the agreement with Ref. 49, where it has been suggested that the optical transitions in tetrahedrally bonded amorphous carbon can be calculated by the convolution of the initial (occupied) and final (empty) states.

To include potential fluctuations due to distorted bonds we consider the σ band density g_σ as an exponential, declining below the energy $E=E_m$ from the parabolic g_Σ band, which is expected for diamond (see Fig. 6). The π -band densities are taken as previously in Eq. (3). So we have for $\epsilon > E_m$,

$$g_{\Sigma^*}(\epsilon) = D(\epsilon - E_{\Sigma^*})^{1/2} \quad (6)$$

and for $\epsilon < E_m$:

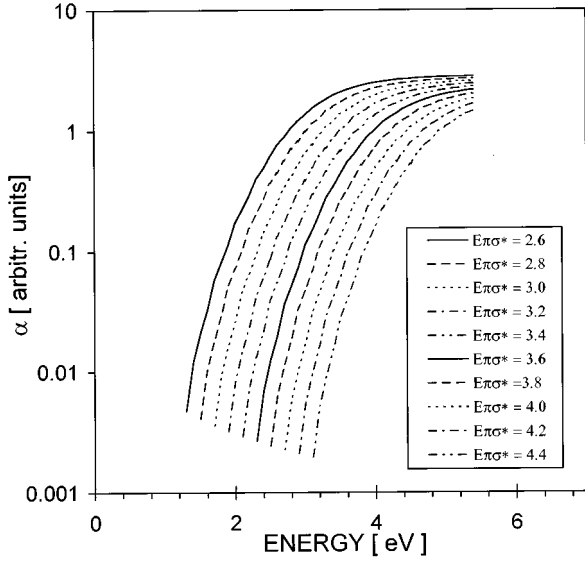


FIG. 9. Numerical calculation of the optical absorption coefficient α due to π - σ^* transitions in amorphous carbon regions, described by Eqs. (6) and (7). Simulations are shown for various energy distances of the π - Σ^* density of states distributions, described by the parameter $E_{\pi\Sigma^*}$, the value for $E_{\pi\pi^*}$ is set to 3.5 eV in these calculations.

$$g_{\sigma} = \{G(E_m - E_{\Sigma^*})^{1/2} / \exp[(E_m - E_{\Sigma^*})/E_1]\} \times \exp[(\epsilon - E_{\Sigma^*})/E_0], \quad (7)$$

where D and G are constants, E_0 is the slope of the exponential tail, and E_{Σ^*} is the bottom of the Σ^* diamond conduction band. The densities described by Eqs. (6) and (7) are equal at $E = E_m$. This gives the preexponential factor in Eq. (7). In this case the convolution integral Eq. (2) can only be solved numerically. The numerical solution of Eq. (2) for various values of E_m and E_1 is shown in Fig. 9. And parameters of the numerical fit are shown in Table II.

C. Indirect transitions in diamond

These transitions are described by a $\alpha \approx (E - E_g \pm E_{\text{ph}})^2$ dependence,²² where E_{ph} is the phonon energy and E_g is the width of the forbidden gap, assuming little change of the matrix elements around the band edges. Such transition cor-

TABLE II. Parameters of the least-squares fitting procedure to Eq. (2) (w , $E_{\pi\pi^*}$, $E_{\pi\Sigma^*}$, E_m , B_1 , B_2 , E_1), described in the Sec. IV and Fig. 6, obtained by a numerical deconvolution of the experimental absorption data.

Sample	w (eV)	$E_{\pi\pi^*}$	$E_{\pi\Sigma^*}$	E_m	B_1	B_2	E_1
d2.1	0.65	3.50	3.89	4.00	95	0.8	0.10
d2.3	0.54	3.07	3.80	3.89	301	0.8	0.10
d2.4	0.57	3.06	3.70	3.80	1017	0.3	0.10
d2.6	0.54	3.00	3.80	3.88	1270	0.4	0.15
d2.7	0.52	3.08	3.70	3.78	1038	0.4	0.10
d2.8	0.47	3.24	3.80	3.89	444	0.2	0.1036
d2.9	0.50	2.90	3.62	3.63	1440	0.2	0.20
D11	0.55	3.40	4.45	4.55	2.4	1.6	0.1

responds to the fundamental absorption in type IIa diamond. As seen in Fig. 1 tailing off of the optical absorption coefficient into the band gap is present. Therefore it is expected that the optical absorption coefficient α is the sum of the indirect transitions between the valence and conduction parabolic bands, and the transitions from the localized states in the broadened exponential tails to states above the band edges:

$$\alpha(E) = G(E - E_g \pm E_{\text{ph}})^2 + H \int g_{\sigma}(\epsilon) g_{\Sigma^*}(\epsilon + E) d\epsilon, \quad (8)$$

where G and H are constants, E_g is the fundamental indirect gap, g_{σ} is the initial density of states, which is approximated by Eqs. (6) and (7), assuming $E_s = E_g$, and g_{Σ^*} is the density of final states above the band edge. It is interesting to note that the calculated absorption spectra according to Eq. (8) for film D11 in Fig. 4 resemble the UV-continuum absorption, present in IIa diamond.⁷ The origin of the continuum absorption has not yet been satisfactorily explained in the literature. It has been suggested that it is connected with the presence of amorphous carbon clusters.⁴⁶

D. Deconvolution of experimental data

The least-squares fitting procedure was used to fit Eq. (2), assuming both π - π^* and π - σ^* transitions, to the experimental values of the optical absorption coefficient, obtained from the PDS measurements. The calculated optical absorption coefficient is plotted together with the experimental data in Figs. 4 and 5. A very good agreement with the experimental data can be established. The parameters of the fit (the preintegration constants B_1 and B_2 , the energy distance $E_{\pi\pi^*}$ between two maxima of the $\pi^{(*)}$ state distributions and their half width at half maximum $2w$, the energy distance $E_{\pi\Sigma^*}$ between the maximum of the π state distribution and the bottom edge of the Σ^* band and the slope E_1 of the exponential broadening of the parabolic Σ band, starting at the energy E_m) are summarized in Table II. In Fig. 8, the relation between the numerically obtained value for the constant B_1 and the measured value of the optical absorption coefficient α at 3.5 eV is plotted. According to these results, by increasing the film quality, the absolute number of π - π^* transitions is decreasing (e.g., lower defect induced optical absorption) and the distance between the two Gaussian distributions (pseudogap) is widening. This is in agreement with data obtained for a -C:H films.

To summarize, the proposed theoretical model describes the character of the characteristic continuum subgap optical absorption in CVD diamond films. The least-square fitting is in a very good agreement with experimental data of the optical absorption spectra for all investigated samples, starting from nanocrystalline films to high-quality CVD diamond.

V. CONCLUSIONS

In this paper, the subgap absorption in CVD diamond films was investigated and a mathematical model for its description developed. The PDS allowed the detailed study of the subgap absorption and the measurement of the optical absorption coefficient in a very broad dynamic range from

$\alpha < 10^{-2} \text{ cm}^{-1}$ to $\alpha > 10^3 \text{ cm}^{-1}$. Based on these data we followed up the development of the main defect structure in CVD diamond from sub-ppm concentration upon changing the deposition conditions.²⁵

Experimental data, presented in Sec. III B showed that all measured CVD films exhibited a very similar feature in the subgap absorption, starting from an onset at about 1 eV. The observed feature resembles the optical absorption spectra of amorphous carbon (*a*-C:H) films, which are believed due to optical transitions in the π - π^* pseudogap.

The morphology study proved that the films with highest subgap absorption were very finely grained with an increased surface of grain boundaries. Raman spectroscopy detected an increased amount of sp^2 carbon in these films. These films were optically smooth (low scattering losses) and optical transmission measurements showed that the characteristic indirect absorption edge of the diamond structure was lost. On the other hand the best-quality CVD diamond attained the character of the fundamental absorption edge, although optical absorption in this region exhibited a broadening. In comparison with absorption data for type Ib (HPHT) diamond and the SIMS analysis²⁵ it has been shown that the characteristic absorption cannot be explained by substitutional ni-

trogen or by other extrinsic impurities.

A numerical deconvolution procedure was developed in Sec. IV D to fit the experimental data, according to the theoretical model. The fit yielded a very good agreement with experimental data and the fitted parameters are very close to those expected from current knowledge of the electronic structure of *a*-C:H.

ACKNOWLEDGMENTS

This work was supported by a NATO International Scientific Exchange Programmes Linkage Grant, Project No. HTECH.LG 940890, and NFWO (Nationaal Fonds voor Wetenschappelijk Onderzoek, Brussels) Research Programme, Project No. G.0014.96 and by the Grant Agency of the Czech Republic, Project No. 202/96/0446. The authors would like to thank E. Sleeks and RUCA in Antwerp for help with optical transmission measurements. The authors appreciate the fruitful discussions with Dr. C. Quaeys, Professor P. Nagels and Dr. S. Kadlec and provision of IIa and Ib diamond plates and homoepitaxial diamond sample by Dr. J. Schermer and Dr. G. Janssen from the University of Nijmegen in The Netherlands.

-
- ¹J.L. Davidson, in *Synthetic Diamond, Emerging CVD Science and Technology*, edited by K.E. Spear and J.P. Dismukes (Wiley, New York, 1994), p. 355.
- ²N.R. Parikh, J.D. Hunn, E. McGucken, M.L. Swanson, C.W. White, R.A. Rudder, D.M. Malta, J.B. Posthill, and R.J. Markunas, *Appl. Phys. Lett.* **61**, 3124 (1992).
- ³B.A. Fox, M.L. Hartsell, D.M. Malta, H.A. Wynands, C.-T. Kao, L.S. Plano, G.J. Tessmer, R.B. Henard, J.S. Holmes, A.J. Tessmer, and D.L. Dreifus, *Diamond Relat. Mater.* **4**, 622 (1995).
- ⁴S.A. Grot, C.W. Hatfield, G. Sh. Gildenblat, A.R. Badzian, and T. Badzian, *Appl. Phys. Lett.* **58**, 1542 (1991).
- ⁵J.A. VonWindheim, V. Venkatesan, D.M. Malta, and K. Das, *J. Electron. Mater.* **22**, 391 (1993).
- ⁶J. Walker, *Rep. Prog. Phys.* **42**, 1605 (1979).
- ⁷C.D. Clark, E.W.J. Mitchel, and B.J. Parsons, in *Properties of Diamond*, edited by J. E. Field (Academic, New York, 1979), p. 22.
- ⁸A. Mainwood, *Phys. Rev. B* **49**, 7934 (1994).
- ⁹P.R. Briddon and R. Jones, *Physica B* **185**, 179 (1993).
- ¹⁰G. Davies and A.T. Collins, *Diamond Relat. Mater.* **2**, 80 (1993).
- ¹¹M. Nesladek, M. Vanecek, J. Rosa, C. Quaeys, and L.M. Stals, *Diamond Relat. Mater.* **4**, 697 (1995).
- ¹²B.V. Deryagin and D.V. Fedoseev, *Growth of Diamond and Graphite from the Gas Phase* (Nauka, Moscow, 1977).
- ¹³K.E. Spear and M. Frenklach, in *Synthetic Diamond, Emerging CVD Science and Technology* (Ref. 1), p. 243.
- ¹⁴W. Piekarczyk, *J. Cryst. Growth* **119**, 345 (1992).
- ¹⁵J. Robertson and E.P. O'Reilly, *Phys. Rev. B* **35**, 2946 (1987).
- ¹⁶J. L. Bredas and G.B. Street, *J. Phys. C* **18**, L651 (1985).
- ¹⁷J. Robertson, *Philos. Mag. B* **66**, 199 (1992).
- ¹⁸R.E. Schroder, R.J. Nemanich, and J.T. Glass, *Phys. Rev. B* **41**, 3738 (1990).
- ¹⁹D.S. Knight and W.B. White, *J. Mater. Res.* **4**, 385 (1989).
- ²⁰J. Tauc, in *Amorphous and Liquid Semiconductors*, edited by J. Tauc (Plenum, New York, 1974).
- ²¹M. Vanecek, J. Kocka, J. Stuchlik, Z. Kozisek, O. Stika, and A. Triska, *Solar Energy Mater.* **8**, 411 (1983).
- ²²G.D. Cody, in *Semiconductors and Semimetals*, edited by J.J. Pankove (Academic, New York, 1984), Vol. 21B, p. 11.
- ²³Xiang Xi Bi, P.C. Eklud, J.G. Zhang, A.M. Rao, T.A. Perry, and C.P. Beetz, Jr., *J. Mater. Res.* **5**, 811 (1990).
- ²⁴M. Vanecek, J. Rosa, M. Nesladek, and L. M. Stals, in *Proceedings of the Diamond '95 Conference, Barcelona, Spain, 11-15 September 1995 [Diamond Relat. Mater.]* (to be published).
- ²⁵M. Nesladek, M. Vanecek, and L.M. Stals, *Phys. Status Solidi A* **154**, 283 (1996), special issue on diamond films.
- ²⁶K. Meykens, M. Nesladek, J.J. Schermer, G. Janssen, M. Vanecek, J. Rosa, L.M. Stals, and C. Quaeys, in *Proceedings of the Diamond '95 Conference* (Ref. 24).
- ²⁷B.A. Fox, B.R. Stoner, D.M. Malta, P.J. Ellis, R.C. Glass, and F.R. Sivazlian, *Diamond Relat. Mater.* **3**, 382 (1994).
- ²⁸C. Wild, R. Kohl, N. Herres, W. Muller-Sebert, and P. Koidl, *Diamond Relat. Mater.* **3**, 373 (1994).
- ²⁹R.G. Buckley, T.D. Moustakas, Ling Ye, and J. Varon, *J. Appl. Phys.* **66**, 3595 (1989).
- ³⁰L. Bergmann, B.R. Stoner, K.F. Turner, J.T. Glass, and R.J. Nemanich, *J. Appl. Phys.* **73**, 3951 (1993).
- ³¹L. Bergmann, M.T. McClure, J.T. Glass, and R.J. Nemanich, *J. Appl. Phys.* **76**, 3020 (1994).
- ³²P.J. Fallon and L.M. Brown, *Diamond Relat. Mater.* **2**, 1004 (1993).
- ³³W. Jackson, N.M. Amer, A.C. Boccara and D. Fournier, *Appl. Opt.* **20**, 1333 (1981).
- ³⁴N.M. Amer and W.B. Jackson, in *Semiconductors and Semimetals*, (Ref. 22), p. 83.
- ³⁵H. Curtins and M. Favre, in *Amorphous Silicon and Related Materials*, edited by H. Fritzsche (World Scientific, Singapore, 1989), p. 328.

- ³⁶E. Gheeraert, A. Deneuville, E. Bustarret, and F. Fontaine, *Diamond Relat. Mater.* **4**, 684 (1995).
- ³⁷H.R. Philipp and E.A. Taft, *Phys. Rev.* **136**, A1445 (1964).
- ³⁸C. Agnus, M. Sunkara, S.R. Sahaida, and J.T. Glass, *J. Mater. Res.* **7**, 3001 (1992).
- ³⁹P.A. Bachmann, D. Leers, and H. Lydtin, *Diamond Relat. Mater.* **1**, 1 (1991).
- ⁴⁰M.A. Tamor and M.P. Everson, *J. Mater. Res.* **9**, 1839 (1994).
- ⁴¹R.S. Sussmann, J.R. Brandon, G.A. Scarsbrook, C.G. Sweeney, T.J. Valentine, A.J. Whithead, and C.J. Wort, *Diamond Relat. Mater.* **3**, 303 (1994).
- ⁴²N. Savvides, *J. Appl. Phys.* **58**, 518 (1985).
- ⁴³Y. Bounouh, M.L. Theye, A. Dehbi-Alaoui, A. Matthews, J. Cernogora, and J.L. Fave, C. Colliex, A. Gheorgiu, and C. Senemaud, *Diamond Relat. Mater.* **2**, 259 (1993).
- ⁴⁴K. Okumura, J. Mort, and M. Machonkin, *Philos. Mag. Lett.* **65**, 105 (1992).
- ⁴⁵H.C. Van De Hulst, *Light Scattering by Small Particles* (Wiley, New York, 1957).
- ⁴⁶C.D. Clark, R.W. Ditchburn, and H.B. Dyer, *Proc. R. Soc. London A* **237**, 75 (1956).
- ⁴⁷S. Abe and Y. Toyazawa, *J. Phys. Soc. Jpn.* **50**, 2185 (1981).
- ⁴⁸W.B. Jackson, S.M. Kelso, C.C. Tsai, J.W. Allen, and S.-J. Oh, *Phys. Rev. B* **31**, 5187 (1985).
- ⁴⁹N. A. Marks, D. R. McKenzie, B. A. Pailthorpe, M. Bernasconi, and M. Parrinello, *Phys. Rev. Lett.* **76**, 768 (1996).
- ⁵⁰U. Stephan, Th. Frauenheim, P. Blaudeck, and G. Jungnickel, *Phys. Rev. B* **50**, 1489 (1994).
- ⁵¹C.Z. Wang, K.M. Ho, and C.T. Chan, *Phys. Rev. Lett.* **70**, 611 (1993).
- ⁵²D.A. Drabold, P.A. Fedders, and P. Stumm, *Phys. Rev. B* **49**, 16 415 (1994).
- ⁵³Ch.H. Lee, W.R.L. Lambrecht, B. Segall, P. C. Kelires, T. Frauenheim, and U. Stephan, *Phys. Rev. B* **49**, 11 448 (1994).
- ⁵⁴J. Robertson, *Diamond Relat. Mater.* **4**, 297 (1995).
- ⁵⁵V.S. Veerasamy, G.A.J. Armatunga, W.I. Milne, P. Hewitt, P.J. Fallon, D.R. McKenzie, and C.A. Davis, *Diamond Relat. Mater.* **2**, 782 (1993).